# Measurement of complete Auger electron emission angular distributions from $\beta$-SiC films on Si(100)

Oliver M. R. Chyan, Douglas G. Frank, and Arthur T. Hubbard
*Surface Center and Department of Chemistry, University of Cincinnati, Cincinnati, Ohio 45221-0172*

J. P. Li and Andrew J. Steckl
*Nanoelectronics Laboratory, Department of Electrical and Computer Engineering, University of Cincinnati, Cincinnati, Ohio 45221-0030*

(Received 6 July 1993; accepted 30 October 1993)

The structure of epitaxial $\beta$-SiC thin films grown on Si(100) has been investigated by measuring Auger electron emission angular distributions over an essentially complete hemisphere of angles of emission above the film surface. The $\beta$-SiC films were grown by rapid thermal chemical vapor deposition, in which the heated Si(100) surface was carbonized with propane. Auger emission angular distributions were measured for carbon at 268 eV, and for silicon at 86 and 1605 eV, allowing the film structure to be probed from the viewpoint of each element. The Auger measurements probe the film structure to a depth of several atomic layers. Each of the distributions displayed distinct, fourfold symmetric features, demonstrating the crystalline character of the $\beta$-SiC films. Comparison of the measured angular distributions with geometric projections and simulations for the known $\beta$-SiC structure indicates that the films consist of interspersed [100] crystalline domains (each domain having twofold symmetry), with 90° in-plane rotational orientations between domains. These findings are consistent with scanning tunneling microscopy observations of the outermost atomic layer.

## I. INTRODUCTION

SiC-on-Si heteroepitaxy provides an attractive combination of two semiconductors.[1] By virtue of its wide bandgap and refractory properties, SiC can extend silicon technology into novel applications.[1,2] The surface characteristics of SiC films grown on silicon strongly influence eventual device performance and thus merit investigation. Previous reports[3,4] include SiC surface studies employing low-energy electron diffraction (LEED), high-resolution electron energy loss spectroscopy (HREELS), Auger electron spectroscopy (AES), and more recently scanning tunneling microscopy (STM).[5-7] The first STM atomic-scale imaging reported[7] of the surface of SiC-on-Si thin films indicated an unreconstructed (1×1) structure in the regions examined. While capable of atomic resolution, STM provides primarily a highly localized contour map of the outermost surface layer. Accordingly, direct evidence concerning the bulk structure of the film must be obtained by means of a complementary method. Reported here are the first investigations of the structure of SiC-on-Si thin films by means of complete Auger electron emission angular distributions.

Auger electron emission angular distributions are finding increased use as a means by which to probe the surface region of a solid, and are particularly useful when the surface under study exhibits some degree of long-range order. Several investigations employing complete Auger emission angular distributions from ordered samples have been reported recently, including studies of monoatomic layers, multilayers and thin films, and single crystals.[8-18] Although the results of these investigations surprised some workers,[13,14,16,17] the experimental trends are becoming established. For example, Auger electron emission angular distributions from single-crystals contain intensity minima along internuclear directions at low kinetic energy (KE < 100 eV), while displaying maxima along internuclear directions at higher KE (> 300 eV).[9] In contrast, angular distributions measured from monolayers and thin films contain intensity minima along internuclear directions at all KEs investigated.[10-12] The fact that these results were not expected by many workers illustrates the need for more realistic theoretical formalisms of electron scattering, and indeed, several new theoretical approaches have been offered recently.[16-18] Although significant theoretical work remains to be done in order to arrive at formalisms which quantitatively relate these measured Auger electron angular distributions to surface crystallographic structure, the distributions are still useful on a qualitative level, as illustrated in this work. Specifically, the symmetry and geometric arrangement of atoms in the first several atomic layers near the solid surface are directly expressed in the distributions. This work illustrates the utility of such measurements when combined with other surface-structure sensitive probes.

## II. EXPERIMENT

$\beta$-SiC films were grown on $n$-type Si(100) wafers using rapid thermal chemical vapor deposition (RTCVD) at atmospheric pressure. The RTCVD technique utilized continuous gas flow of appropriate precursors in conjunction with the rapid heating and cooling capability of low thermal mass rapid thermal processing (RTP) equipment to control the growth process. In RTCVD, growth takes place only during the limited period when the system is at high temperature, thus combining high quality thin film growth with very abrupt interfaces between thin films of various materials. Epitaxial growth of crystalline cubic $\beta$-SiC on Si(100) by RTCVD has been reported recently.[19] For these experiments,

 ©1994 American Vacuum Society 

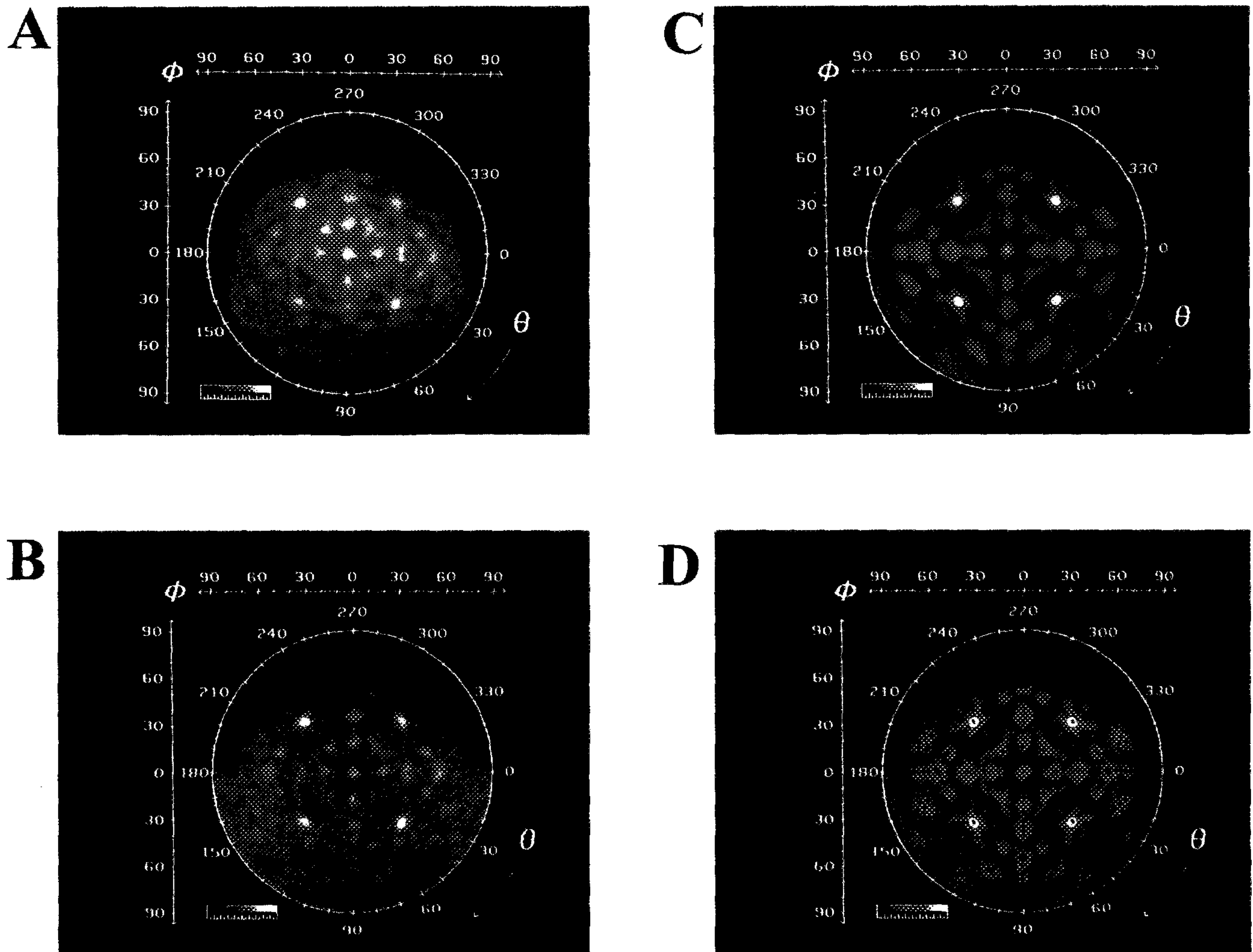


FIG. 1. (A) Angular distribution of 1605 eV silicon Auger electrons emitted from the β-SiC film. Brighter colors (white, yellow) represent stronger Auger signals as illustrated in the color intensity bar (see color scale, lower left). The center of the image corresponds to emission normal to the surface and the edge of the image corresponds to grazing emission, as illustrated by the angular scales included with each image. (B) Background-subtracted 1605 eV distribution. (C) Background-subtracted and fourfold symmetry-averaged 1605 eV distribution. (D) 1605 eV distribution with geometric projection of β-SiC structure [see Fig. 4(B)].

SiC films were grown by carbonization of the silicon surface through reaction with propane in a hydrogen ambient. A typical growth procedure consists of *in-situ* cleaning with a mixture of HCl and $H_2$, followed by carbonization at temperatures from 1100 to 1300 °C in the presence of $C_3H_8$ and $H_2$ carrier gas. A more detailed description of the growth process can be found in Ref. 19. The SiC films used in this study had a thickness in the range of 10–100 nm. X-ray diffraction (XRD) and LEED confirmed that the films had a cubic [100] oriented structure.

The apparatus used for the Auger electron angular distribution measurements has been described previously.[8,15] In this work, Auger emission was stimulated by an incident electron beam impinging on the sample at a fixed angle of 11° from the surface plane. The incident beam and sample remained stationary while the moving analyzer scanned the angles comprising the complete forward hemisphere above the solid surface. Electron emission along trajectories selected by the analyzer was angle-resolved with collimating apertures. The selected electrons were then energy-resolved, modulated by means of electrostatic lenses, and then synchronously amplified in order to distinguish the Auger signal from background signals. A 20 $mm^2$ portion of the sample was irradiated with a 10 $\mu$A beam at 2 keV; the area analyzed was approximately one square millimeter. For measurements of relatively high kinetic energy Auger electrons (1605 eV), a 15 $\mu$A beam at 6 keV was used. A small portion of the angular distribution was inaccessible to allow for the incident beam, and the experimental geometry was such that the analyzed area increased with polar angle.[11] Each final angular distribution contains 27 331 data points, affording 1° resolution. The β-SiC samples were also characterized by LEED and AES before and after the angular distribution measurements to verify surface structure and stability.

## III. RESULTS AND DISCUSSION

Complete Auger electron emission angular distributions were measured from the β-SiC film for three Auger transitions: carbon at 268 eV (primarily $KL_{2,3}L_{2,3}$), silicon at 86

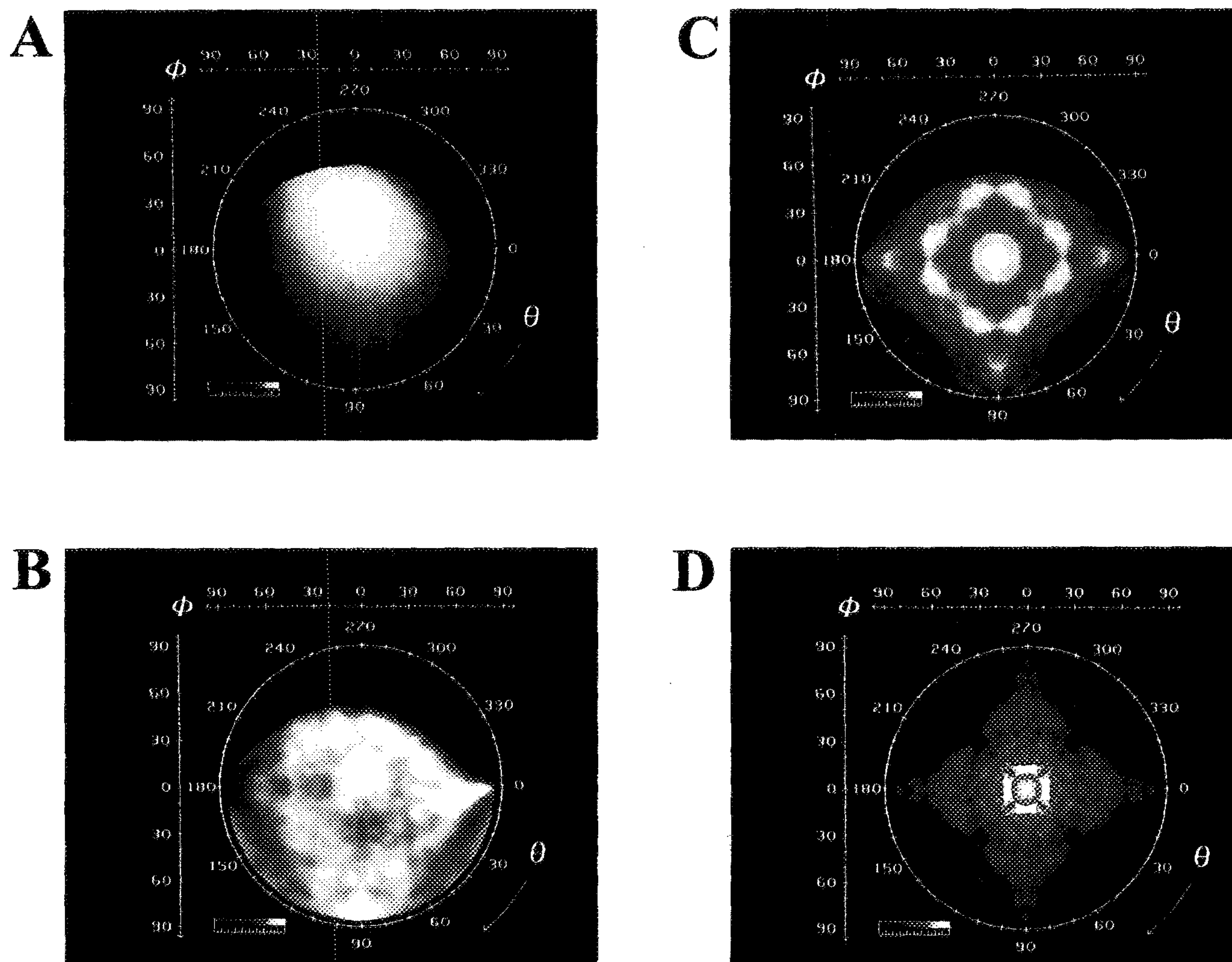


FIG. 2. (A) Angular distribution of 86 eV silicon Auger electrons emitted from the $\beta$-SiC film. (B) Background-subtracted 86 eV distribution. (C) Background-subtracted and fourfold symmetry-averaged 86 eV distribution. (D) Simulation of the 86 eV angular distribution for silicon.

eV (primarily $L_3M_{2,3}M_{2,3}$), and silicon at 1605 eV (primarily $KL_2L_3$ and $KL_3L_3$). The complete distributions for each energy are shown in Figs. 1(A), 2(A), and 3(A) as false-color intensity maps, where brighter colors (white, yellow) represent larger measured Auger signals and darker colors (black, blue) represent smaller ones. For each distribution, the data were normalized such that the left edge of the intensity scale (graduated scale at lower left) corresponds to zero measured signal, while the right edge corresponds to the maximum observed Auger signal. Also, the color bars were normalized over each data range to enhance the contrast of the images. The distributions are displayed in spherical coordinates, where $\phi$ and $\theta$ are the polar and azimuthal coordinates, respectively. The center of the image corresponds to $\phi=0°$ (the surface normal) and the edge of the image corresponds to $\phi=90°$ (grazing emission). As illustrated by the coordinate axes included with each display, $\phi$ varies in a linear fashion from the center to the edge of the image.

In addition to a color map of the raw data for each energy, a "background-subtracted" image is provided for each energy to facilitate the viewing of distribution features. The background for each distribution was calculated as follows: for each direction of emission $(\theta,\phi)$, a background value was obtained by digitally averaging a large group of adjacent data points ($\theta=\pm 20°$, $\phi=\pm 20°$). This process generates an empirical distribution which is featureless except for gradual variations. Subtraction of the background increases the contrast of the distribution, does not introduce any new features into the distribution, and reduces contributions such as those due to the angular variations of the analyzer field of view (analyzer sensitivity function). To further enhance fine features in the distributions, a symmetric averaging process is applied, employing the observed symmetry of the images. These highly processed images are not intended to replace the raw images, but to be used in conjunction with and to facilitate interpretation of the raw data.

### A. High kinetic energy Kikuchi pattern (1605 eV)

The measured angular distribution of 1605 eV electrons emitted from the $\beta$-SiC film is shown in Fig. 1(A). Background-subtracted, and background-subtracted symmetry-averaged images are provided in Figs. 1(B) and 1(C). Clearly visible in the data is a fourfold pattern of intensity maxima (white/yellow spots) which correlates well

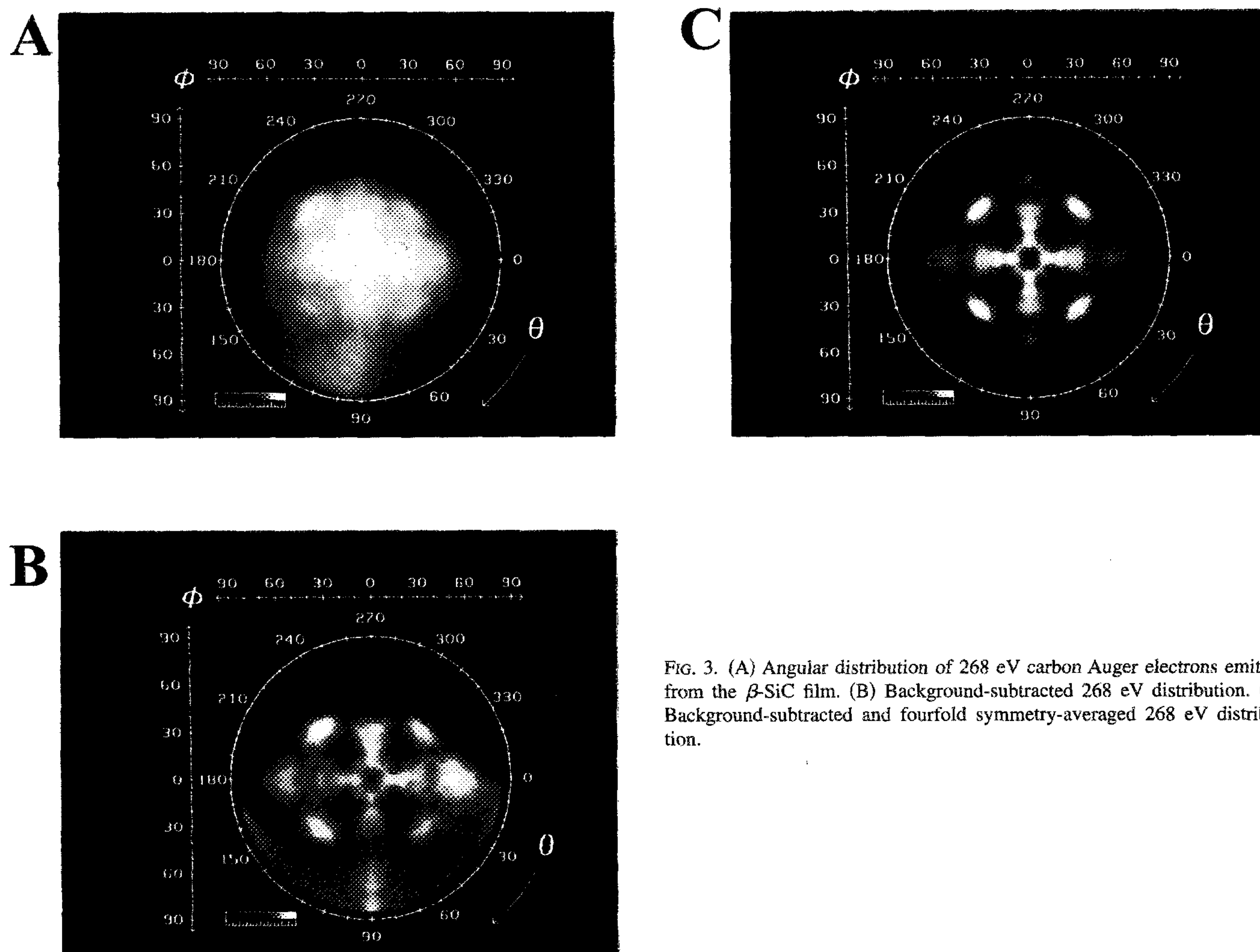


FIG. 3. (A) Angular distribution of 268 eV carbon Auger electrons emitted from the $\beta$-SiC film. (B) Background-subtracted 268 eV distribution. (C) Background-subtracted and fourfold symmetry-averaged 268 eV distribution.

with a geometric projection of the known structure of $\beta$-SiC, Fig. 1(D) and Fig. 4. This phenomenon is often referred to as a "Kikuchi pattern," [20] or equivalently as an "electron channeling" [21] pattern, and is the result of incoherent, inelastic scattering of Auger electrons emitted from within the bulk of the film by long rows of atoms in the lattice.[22] Such data are useful for probing the overall symmetry and orientation of the film to a depth of about 10 nm. In this case, the fourfold symmetry of the pattern confirms that the film is crystalline, and that the film is rotationally oriented with respect to the Si(100) substrate. This fact is clearly illustrated in Fig. 1(D), in which a geometric projection for the $\beta$-SiC structure [Fig. 4(B)] is superimposed upon the image shown in Fig. 1(C). The geometric projection shown in Fig. 4(B) was calculated for eight atomic layers of $\beta$-SiC by placing "dots" in the distribution along trajectories corresponding to the interatomic axes. Larger dots refer to closer interatomic distances, while smaller dots correspond to more distant interatomic relationships. Since the closest interatomic directions are often parallel to the clearest channels through a crystalline film, there is an approximate correlation between the size of a dot and the observed intensity in the distribution [Fig. 1(D)].

### B. Low kinetic energy Si Auger electrons (86 eV)

The measured angular distribution of silicon Auger electrons (86 eV) emitted from the $\beta$-SiC film is shown in Fig. 2(A). In contrast to the sharp fourfold pattern exhibited in the high KE distribution [Fig. 1(A), 1605 eV], the features of the low KE distribution [Fig. 2(A), 86 eV] are much weaker relative to the instrument response function and other background effects. Accordingly, the features of the 86 eV distribution are difficult to view without background subtraction and fourfold symmetric averaging, Figs. 2(B) and 2(C). The relative degree of angular anisotropy in the measured angular distributions can be seen more quantitatively in polar plots extracted from the complete distributions.

Comparison of the high and low KE results for silicon (Figs. 1, 2, and 5) reveals that, in general, the intensity maxima apparent along internuclear directions at high KE have been replaced by intensity minima at the low KE. This result is consistent with the trend observed for elemental single-crystals[15,18] and is illustrated in Fig. 6. Shown are $\phi=45°$ azimuthal plots extracted from the complete distributions shown in Figs. 1(C), 2(C), and 3(C). In Fig. 6, the nearest-neighbor interatomic directions for $\beta$-SiC(100) are indicated by vertical dashed lines in the $\theta=45°$, 135°,

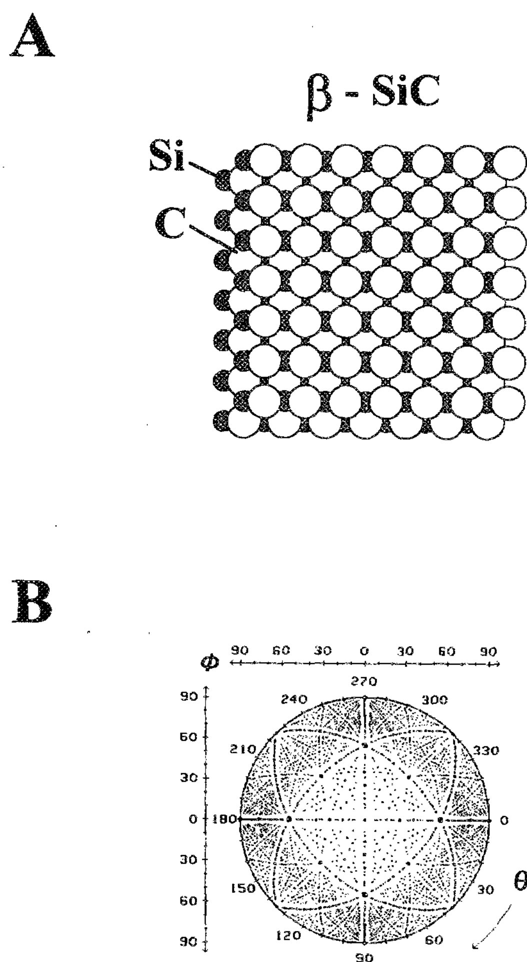


FIG. 4. (A) Top-view model of the β-SiC structure. Note that the elemental geometry has only twofold symmetry. (B) Geometric projection for eight atomic layers of β-SiC. Each dot represents an internuclear direction in the structure; larger dots refer to closer internuclear spacings.

225°, and 315° azimuthal directions. One obvious exception to the above trend occurs along the surface normal (the center of the images), where intensity maxima are observed for both high and low KE. However, the presence of an intensity maximum along the surface normal at low KE is not an exception to the trend, since the carbon atoms located in the atomic layer above each emitting silicon atom are not directly above the emitter, but are offset, leaving a "gap" through which an Auger electron may pass with less probability of being inelastically scattered [Fig. 4(A)]. In other words, an intensity minimum is not observed along the surface normal because the surface normal is not an internuclear direction for most of the emitting atoms near the surface; that is, most of the Auger electrons detected at low KE originate from the outermost atomic layers due to the short inelastic mean-free path. At high KE, the mean-free path is much longer, which emphasizes the channels through the crystal rather than the local arrangement of atoms surrounding each emitting atom.

As a step toward a more quantitative description of the relative intensities of features in low KE distributions, we have developed a straightforward empirical formalism based

TABLE I. Unit cell structural parameters for the β-SiC bilayer.[a]

| Element | Relative coordinates (Å) | | |
|---|---|---|---|
| | $x$ | $y$ | $z$ |
| Si | 0.0 | 0.00 | 0.00 |
| | 1.54 | 1.54 | 2.18 |
| C | 1.54 | 0.00 | 1.09 |
| | 3.08 | 1.54 | 3.27 |

[a]The SiC bond distance was 1.94 Å. The simulation scattering parameters were as follows: $T_{Si}=0.6$, $T_C=0.6$, $r_{Si}=0.8$ Å, $r_C=1.2$ Å.

upon point-emitters and spherical scatterers of Auger electrons. For a known structure, the formalism has only two variable parameters: the effective scattering radius of the atoms, and the scattering probability. Thus, the relative Auger intensity predicted along a given trajectory depends only upon the number of scattering atoms located between each emitting atom and the detector. Despite the simplicity of this empirical formalism, it has been successful at predicting the qualitative features of angular distributions for a wide variety of samples, including single-crystals, monoatomic layers, and thin films.[8–15] Since the empirical formalism predicts intensity minima along internuclear directions due to blocking of Auger electrons, it works best for monolayers, thin films, and single crystals at low KE (<100 eV) (channeling effects predominate in single-crystal distributions for KEs > 300 eV). The KE of the Auger electron is less important in the case of monolayers and thin-films, since there are fewer atoms located between the emitting atoms and the detector. This emphasizes the scattering due to atoms neighboring the emitting atom, and reduces the probability that an emitted electron will encounter long rows (i.e., channels) of atoms.

A simulated angular distribution of Auger electrons (86 eV) emitted from the β-SiC film is shown in Fig. 2(D). The structural model used for the simulation consisted of 11×11 unit cells of β-SiC, 16 atomic layers deep (a total of 1936 atoms). The simulation was fourfold symmetry averaged to facilitate comparison with Fig. 2(C). The structural parameters employed for the simulation are collected in Table I. The simulation predicts the presence of an intensity maximum normal to the surface (the center of the image), in agreement with experiment. The simulation also predicts several other features of the distribution, including the broad attenuations near grazing emission ($\phi > 60°$) located at $\theta = 45°$, 135°, 225°, and 315° which give the background-subtracted images [Figs. 2(B) and 2(C)] a pincushion ("⌘") shape. This pronounced feature of the distribution is attributable to the increasing number of scattering atoms (i.e., increasing path length) which the emitted electrons encounter as grazing angles of emission are approached [see Fig. 2(D)]. Although the relative intensities of the simulated features are not precisely identical to the measured ones, the simulation indicates that the structure of the SiC film near the surface is essentially the same as that of bulk β-SiC. That is, the relative positions of atoms are revealed more by the locations of features in the distribution than by their absolute intensities.

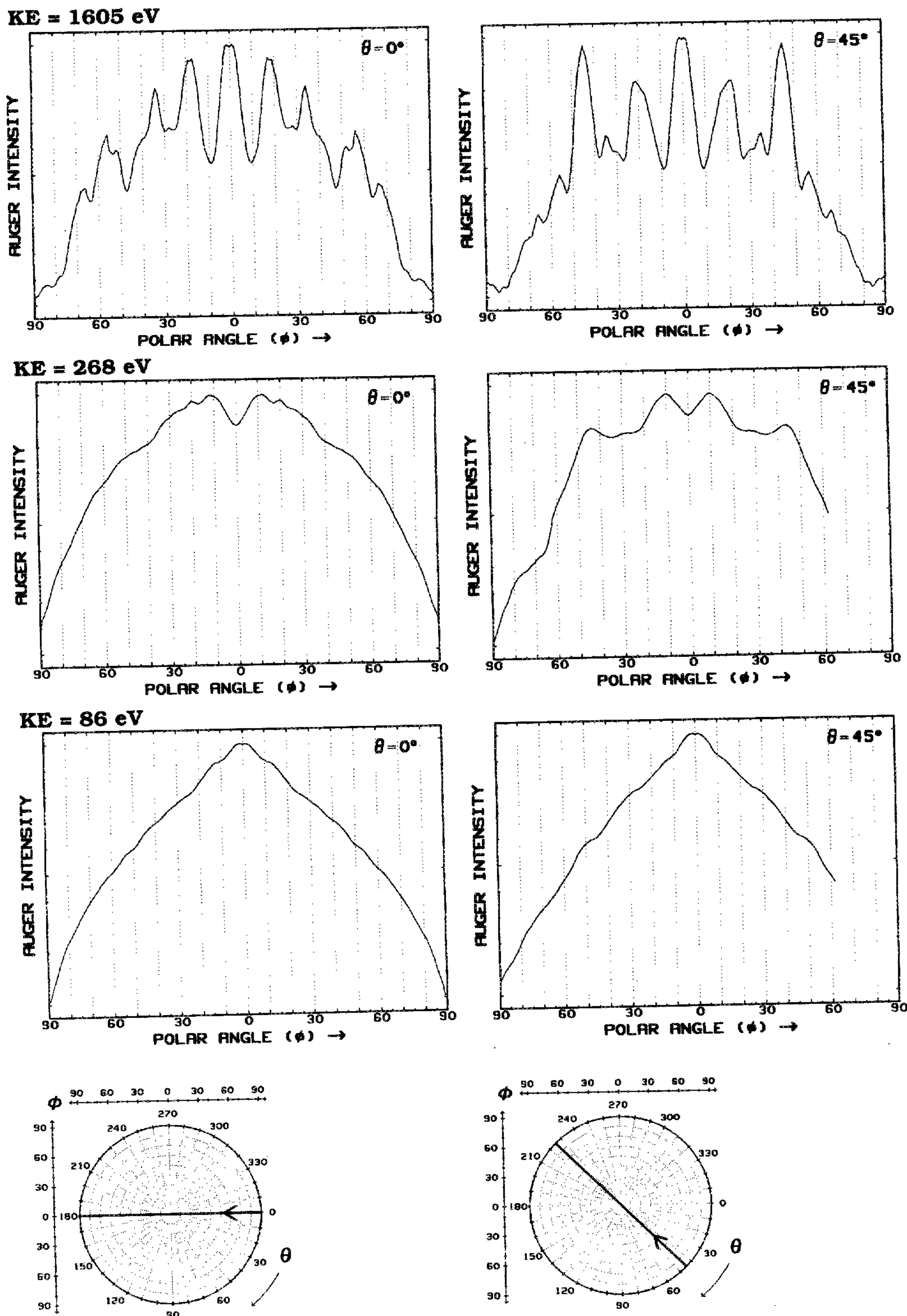


FIG. 5. Polar plots extracted from the complete measured angular distributions for Si (86 eV, 1605 eV) and C (268 eV). The polar plots were extracted along coordinates illustrated at the bottom of each column of plots. The angular anisotropy of emission from the $\beta$-SiC surface increases with kinetic energy, due to channeling of Auger electrons emitted from atoms located more deeply in the bulk of the film.

### C. Intermediate kinetic energy C Auger electrons (268 eV)

The measured angular distribution of carbon Auger electrons emitted from the $\beta$-SiC film is shown in Fig. 3(A). Features in the distribution are sharper than those observed for silicon at low KE [Fig. 2(A)], but are less sharp than the channeling features observed in the high KE angular distribution for silicon [Fig. 1(A)]. In fact, the 268 eV image contains features similar to both the high and low KE images, appearing to contain a mixture of both channeling and

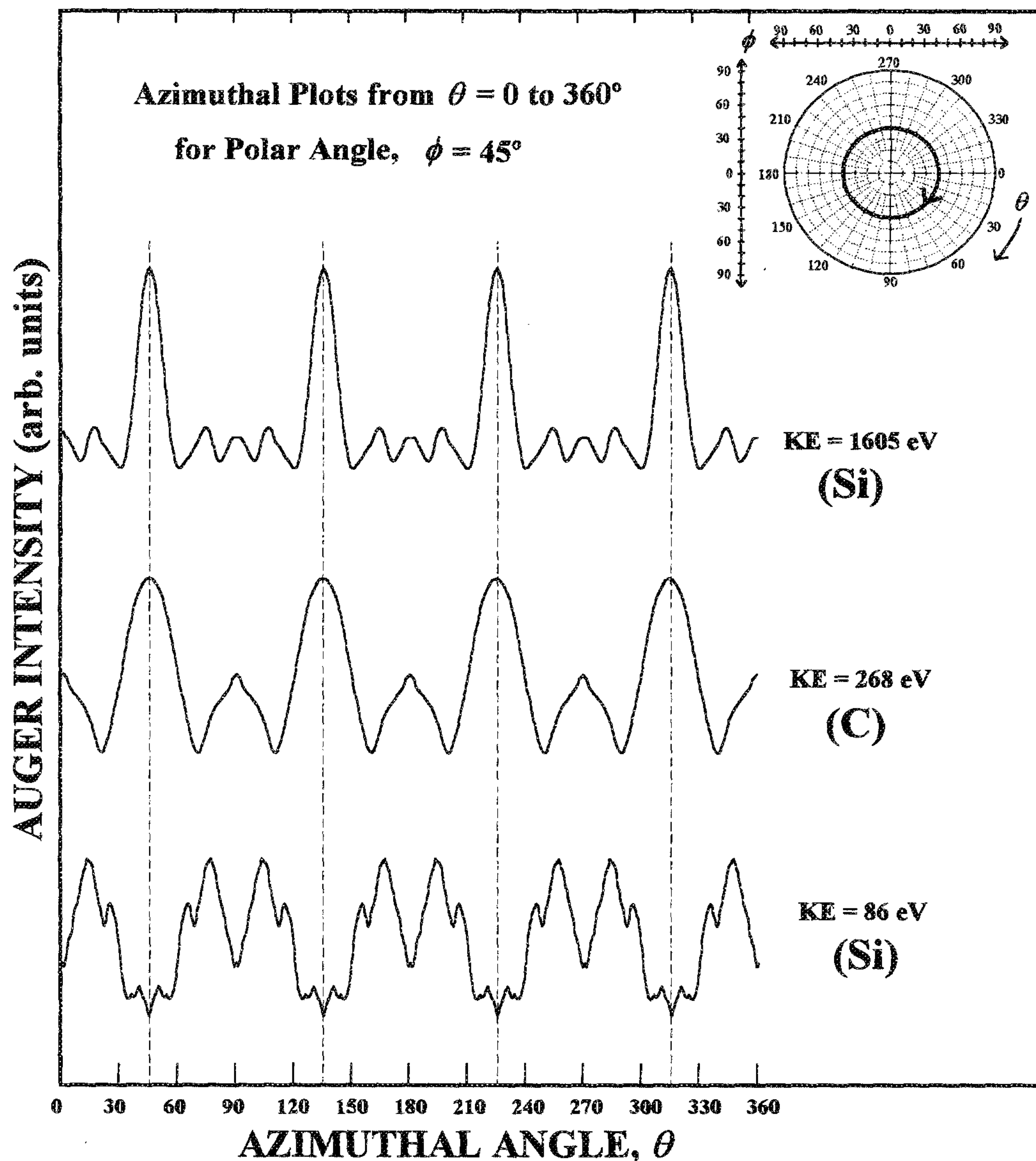


FIG. 6. Azimuthal plots extracted from the complete angular distributions shown in Figs. 1(C), 2(C), and 3(C). The coordinates along which the data were extracted are illustrated in the diagram located at the upper right. The vertical dashed lines which pass through the plots indicate the nearest-neighbor directions in the β-SiC single-crystal. The plots illustrate the trend observed for many single-crystal samples, in which intensity maxima observed along internuclear directions at high KE are replaced by intensity minima at low KE.

blocking effects. This finding is consistent with the behavior observed for several single-crystal samples, in which intensity minima present along internuclear directions at low KE (<100 eV) gradually gave way to intensity maxima at higher KE (>300 eV).[9] For example, intensity minima present along the Si-C nearest-neighbor directions ($\phi$=45°; $\theta$=45°, 135°, 225°, 315°) at low KE (Fig. 2, 86 eV) are replaced by intensity maxima in the carbon (Fig. 3, 268 eV) and silicon (Fig. 1, 1605 eV) distributions. This behavior is also apparent in Fig. 6. As observed for single-crystals,[18] these channeling maxima are the most pronounced since the nearest-neighbor axes also correspond to the clearest channels through the crystal. The broad attenuations apparent near grazing emission at the low KE are retained in the intermediate KE image (giving the image its overall pincushion shape), which suggests that the mean-free path is still much smaller than that observed at higher KE.

The intensity minimum observed along the surface normal in the intermediate KE distribution was not observed in the low or high KE distributions. This can be understood in terms of the fact that, as for the other KEs, the presence of maxima and minima in the distributions depends upon the relative degree of blocking and channeling which is occurring along each trajectory. Since the surface normal corresponds to both a blocking and a channeling direction, predicting the qualitative behavior along this trajectory is more complicated than for the low and high KEs. To illustrate, consider the Auger emission originating from each carbon

atom in the film. If the Auger electron had possessed a low KE (<100 eV), the mean-free path would have been especially short, emphasizing the local geometry surrounding the emitting atom. As illustrated in Fig. 4(A), there is a gap in the atomic layer (Si) located immediately above each emitting carbon atom, so a maximum would be expected at low KE. However, the fourth atomic layer (second C layer) above each emitting carbon atom contains another carbon atom which is located directly above the emitting carbon atom. Thus, as larger escape depths occur due to increasing KE, the maximum observed due to the gap in the adjacent layers will be gradually replaced by a minimum due to blocking by alternate layers, then by third layers, and so on, until channeling features finally predominate at higher KE. Because of the large number of interatomic relationships and scattering mechanisms which are occurring at intermediate KE, such behavior is quite complicated to simulate. A complete quantum mechanical description of such data is beyond the scope of this work, and is the focus of an ongoing effort.

The complex mixture of channeling and blocking features present in intermediate KE angular distributions makes interpretation of such data less straightforward than for the low or high KE data for direct determination of surface atomic structure of thick samples (more than several atomic layers). However, depending upon the KE (and the corresponding mean-free path), such distributions provide supporting evidence regarding the average structure in the outermost several atomic layers. In this case, the intermediate KE data confirm that the β-SiC film is crystalline, and that the structure of the outermost several atomic layers of the film is contiguous with that of the bulk.

## IV. SUMMARY AND CONCLUSIONS

Three complete Auger electron emission angular distributions measured from a β-SiC film were presented here: two for silicon Auger electrons (86 and 1605 eV), and one for carbon Auger electrons (268 eV). Each distribution displays fourfold symmetry, despite the twofold symmetry of β-SiC, indicating that the film consists of two structural domains rotated 90 ° with respect to each other. Also evident in each distribution are distinct features which correspond to the expected interatomic directions of β-SiC, indicating that a crystalline film was formed which is rotationally aligned with the Si(100) substrate, and which possesses the known cubic structure of β-SiC. These results corroborate earlier STM measurements for the same film,[7] while providing direct, complementary evidence regarding the bulk of the film.

## ACKNOWLEDGMENTS

This work was supported by the Air Force Office of Scientific Research and the Ohio Edison Materials Technology Center. Instrumentation was provided by the National Science Foundation. The technical assistance of Arthur Case, Frank Douglas, and Richard Shaw, and the generosity of Joan and George Rieveschl, Jr. are gratefully acknowledged.

[1] J. A. Powell and L. G. Matus, in *Amorphous and Crystalline Silicon Carbide*, Springer Series in Physics Vol. 34, edited by G. L. Harris and C. Y-W. Yang (Springer, New York, 1989), pp. 2–12.
[2] R. F. Davis, Z. Sitar, B. E. Williams, H. S. Kong, H. J. Kim, J. W. Palmour, J. A. Edmond, J. Ryu, J. T. Glass and C. H. Carter, Mater. Sci. Eng. B **1**, 77 (1988).
[3] M. Dayan, Surf. Sci. Lett. **149**, L33 (1985).
[4] M. Dayan, J. Vac. Sci. Technol. A **4**, 38 (1986).
[5] N. Z. Zheng, U. Knipping, I. S. Tsong, W. T. Petuskey, H. S. Kong, and R. F. Davis, J. Vac. Sci. Technol. A **6**, 696 (1988).
[6] C. S. Chang, N. H. Zheng, I. S. T. Tsong, Y. C. Wang, and R. F. Davis, J. Vac. Sci. Technol. B **9**, 681 (1991).
[7] A. J. Steckl, S. A. Mogren, M. W. Roth, and J. P. Li, Appl. Phys. Lett. **60**, 1495 (1992).
[8] D. G. Frank, N. Batina, T. Golden, F. Lu, and A. T. Hubbard, Science **247**, 182 (1990).
[9] D. G. Frank, T. Golden, O. M. R. Chyan, and A.T. Hubbard, J. Vac. Sci. Technol. A **9**, 1254 (1991).
[10] D. G. Frank, O. M. R. Chyan, T. Golden, and A. T. Hubbard, J. Vac. Sci. Technol. A **10**, 158 (1992).
[11] D. G. Frank, O. M. R. Chyan, T. Golden, and A. T. Hubbard, J. Phys. Chem. **97**, 3829 (1993).
[12] D. G. Frank, O. M. R. Chyan, T. Golden, and A. T. Hubbard, J. Phys. Chem. (in press).
[13] D. G. Frank, T. Golden, and A. T. Hubbard, Science **248**, 1131 (1990).
[14] D. G. Frank and A. T. Hubbard, Langmuir **6**, 1430 (1990).
[15] D. G. Frank and A. T. Hubbard, in *The Concise Encyclopedia of Materials Characterization*, edited by R. C. Cahn and E. Lifshin (Pergamon, New York, 1993), pp. 34–41.
[16] Y. U. Idzerda and D. E. Ramaker, Phys. Rev. Lett. **69**, 1943 (1992).
[17] T. Greber, J. Osterwalder, D. Naumovic, A. Stuck, S. Hüfner, and L. Schlapbach, Phys. Rev. Lett. **69**, 1947 (1992).
[18] Our theoretical efforts have emphasized measurements for well-known surface structures. Those results indicate that consideration of inhomogeneous inelastic and elastic scattering mechanisms is required. See Refs. 10 and 11 for a more complete discussion.
[19] A. J. Steckl and J. P. Li, IEEE Trans. Electron Devices **ED-39**, 64 (1992).
[20] S. Kikuchi, Jpn. J. Phys. **5**, 83 (1928).
[21] E. G. McRae, Surf. Sci. **44**, 321 (1974).
[22] H. Hilferink, E. Lang, and K. Heinz, Surf. Sci. **93**, 398 (1980).